Structure of the plasma-wall interaction in an oblique magnetic field

E. Ahedo
E.T.S.I. Aeronáuticos, Departamento de Fundamentos Matemáticos, Universidad Politécnica, 28040 Madrid, Spain

(Received 4 April 1997; accepted 9 September 1997)

The influence of the magnetic field strength B and angle of incidence ψ on the one-dimensional (1-D) structure of a weakly collisional plasma near a charged wall is investigated. The models of Chodura [Phys. Fluids **25**, 1628 (1982)] and Riemann [Phys. Plasmas **1**, 552 (1994)] are recovered as particular cases: intermediate-B and weak-B cases, respectively, of the model presented here, and are compared with a third, strong-B case, where the space-charge sheath is partially magnetized. A triple structure comprising (collisional) presheath, Chodura layer, and sheath, exists only for the intermediate-B case. For weaker and stronger ranges of B, the Chodura layer disappears immersed into the presheath and the sheath, respectively, recovering a classical double-structure. In the Chodura model the importance of the collisional presheath to characterize completely the perturbation region is discussed. For the weak-B case: results for the whole range of angles of incidence are presented and compared; for grazing incidence and a near-collisionless plasma, an approximate analytical solution is derived; and, the asymptotic convergence to the triple-structure is shown. For the strong-B case, the analysis includes: (i) an involved derivation of the local behavior around the entrance point to the sheath, and (ii), for a certain range of ψ, to cross, with a regular solution, an internal singular point of the sheath equations. The similarities between the entrance conditions to the different plasma regions are pointed out. © *1997 American Institute of Physics.* [S1070-664X(97)02312-4]

I. INTRODUCTION

The interaction between a weakly collisional plasma (Debye length$\ll$collisional mean free path) and a charged surface has been a subject of interest for many years in areas such as plasma probes, magnetically confined fusion, material processing, and space plasmas. The problem is quite well understood in the absence of a magnetic field. For magnetized plasmas, the anisotropy introduced by the magnetic field makes very difficult the analytical treatment of nonplanar geometries and kinetic models of the plasma, but even the simplest case of a planar geometry and a macroscopic plasma model does not enjoy of a well-established solution yet. Chodura[1] proposed a one-dimensional(1-D), collisionless model where the plasma-wall transition consists of a double structure comprising a quasineutral, ''magnetic presheath'' (here called the Chodura layer) preceding the space-charge (Debye) sheath. The Chodura layer scales with the gyroradius of the attracted species and with the angle of incidence of the magnetic field lines into the wall. Chodura found that the flow had to be sonic/supersonic along the B-field lines at the entrance of the Chodura layer. Consequently, he postulated an additional ''plasma presheath'' (for us, the presheath) where the plasma would be accelerated to sonic conditions.

Grazing incidence: **B** parallel to the wall [$\psi=90°$ in Fig. 1(a)], a degenerate case in Chodura's model, was studied by Behnel (in a work referenced by Riemann[2]) who showed that, if collisions were accounted for, the space-charge sheath could be directly reached from a plasma at rest, without requiring a Chodura layer. Riemann[2] extended this collisional model to oblique magnetic fields and confirmed that collisions provide an adequate transport mechanism to accelerate a quiescent plasma to sonic/supersonic conditions. Although the model of Riemann is valid for any angle of incidence, the numerical results he presents and discusses are restricted to a narrow range of angles close to grazing incidence, $84.3° \leqslant \psi \leqslant 90°$. In the collisionless limit of his model, Riemann's recovers the ''magnetic presheath'' of Chodura but not the ''plasma presheath''; in fact, he asserts that the plasma acceleration cannot be described in that limit, and must be replaced by the ''initial condition'' of a sonic/supersonic flow parallel to the B field.

The entrance conditions to the Chodura layer has deserved the attention of other authors. Stangeby[3] dedicates one paper to discuss what he sees as ''an apparent contradiction'' between the space-charge sheath and the Chodura layer: how can the plasma be supersonic and quasineutral, at the same time, in the Chodura layer. Both Stangeby and Riemann find fundamental differences between the entrance conditions to the Chodura layer and the space-charge sheath; in particular, Stangeby affirms that a singularity in the fluid equations is permitted at the sheath entrance but not at the Chodura layer entrance. The model of the Chodura layer has been extended by Stangeby and Chankin,[4] and Hutchinson[5] to plasmas affected by an additional $\mathbf{E}\times\mathbf{B}$ drift caused by an external electric field, parallel to the wall and superimposed to the self-consistent one created by the wall potential. On the contrary, no detailed analysis of the collisional presheath has been found. This analysis would give a clear description of the transition to the Chodura layer, and would allow us to compare the roles of the presheath and the Chodura layer. Experimental results that show the interaction of magnetic and collisional effects on the quasineutral plasma have been presented by Kim *et al.*[6]

The models of Chodura and Riemann assume that the space-charge sheath is unmagnetized. When the magnetic

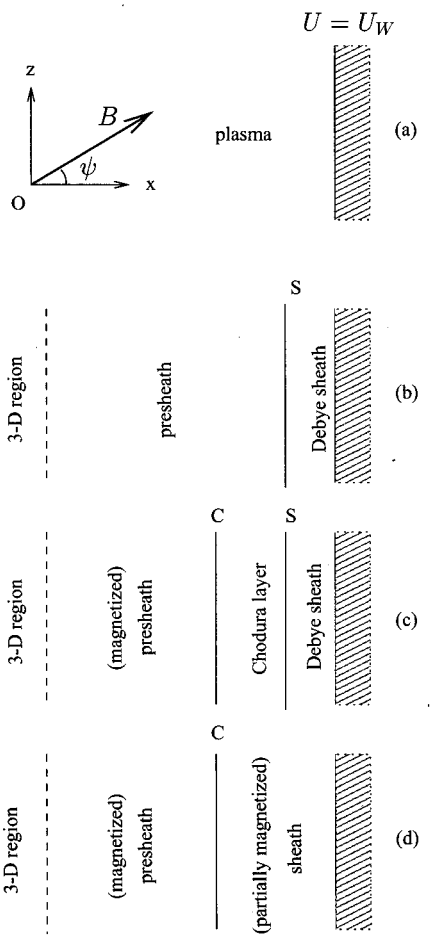

FIG. 1. (a) Reference frame used in the model and angle of incidence of **B**; Oxz is the plane of incidence. Sketches of the plasma structure for (b) weak, (c) intermediate, and (d) strong B field. In each case, the transition points, C or S, marked in the figures are well defined: they are singular/sonic points of the plasma equations. The transition to the 3-D region, not discussed here, is not well defined in the 1-D model.

field is strong enough, this hypothesis is no longer valid. The coupling between space-charge and magnetic effects was treated marginally by Chodura. Daybelge and Bein[7] investigated a magnetized sheath at angles close to grazing incidence with a kinetic model. DeWald *et al.*[8] simulated obliquely magnetized sheaths with particle-in-cell techniques. Grazing incidence in a cold-plasma sheath was studied by Tao *et al.*[9] but their model lacks consistency because they took the space-charge field as an input function.

In this paper we present a model of the evolution of the complete 1-D perturbed region in the entire range of magnetic field strength and angle of incidence. The models of Chodura, Riemann, and partially magnetized sheaths are obtained as particular cases of that general model at different asymptotic limits of B. Section II presents the model and its basic properties. Section III completes the model of Chodura with the inclusion of the ''plasma presheath,'' and a comparative discussion of the three plasma regions. Section IV is dedicated to the model of Riemann. Section V analyzes the structure of partially magnetized sheaths for strong B fields. Conclusions are presented in Sec. VI.

II. FORMULATION OF THE MODEL

In a Cartesian reference frame $Oxyz$, Fig. 1(a), the perfectly absorbing wall is placed at $x=x_W$ (the value of x_W is irrelevant) and the plasma occupies the region $x<x_W$. The wall is biased to an electric potential $U=U_W$, relative to the plasma potential (at a certain reference point) far enough from the wall but still in the 1-D region; $|U_W|$ is assumed large enough to form a space-charge sheath close to the wall. Since, independently of the sign of U_W, it is $qU_W<0$, where q is the electric charge of the attracted species, cathodic and anodic walls will be treated simultaneously. The plasma is magnetized by an external, uniform magnetic field,

$$\mathbf{B}=B(\mathbf{1}_x \cos\psi+\mathbf{1}_z \sin\psi),$$

where B and ψ are defined such that $qB>0$. The one-dimensional, steady-state solution will depend on the the plasma parameters, U_W, ψ, and B. The self-consistent electric field, $\mathbf{E}(x)=-\mathbf{1}_x dU/dx$, will be part of the solution.

Plasma dynamics are modeled by the following set of equations:

$$\frac{d^2U}{dx^2}=4\pi q(N_r-N), \tag{1}$$

$$T_r \ln N_r - qU = \text{const}, \tag{2}$$

$$NV_x=\Gamma_{x\infty} \quad (\text{const}), \tag{3}$$

$$mV_x\frac{d\mathbf{V}}{dx}=q\mathbf{V}\times\mathbf{B}-\left(q\frac{dU}{dx}+\frac{T}{N}\frac{dN}{dx}\right)\mathbf{1}_x-\nu_c m\mathbf{V}, \tag{4}$$

where m, q, N, T, and $\mathbf{V}=(V_x,V_y,V_z)$, are the mass, electric charge, density, temperature, and velocity of the attracted species, respectively; $-q$, N_r, and T_r, are the electric charge, density, and temperature of the repelled species (there is no macroscopic flow of the repelled species); and ν_c is the effective collision frequency. Collisions are included to provide a mechanism that can accelerate the 1-D, quiescent plasma; the particular processes that define ν_c are not discussed in this paper, and we simply assume that ν_c is constant. Collection of particles of the repelled species and secondary emissions are disregarded. In order to stand out the essential features of the plasma response, simple, isothermal laws have been assumed for both plasma species. The continuity equation (3) expresses that all particles that enter the 1-D region are absorbed by the wall, but the particle flow $\Gamma_{x\infty}$ is a free parameter of this 1-D model that would be determined by matching the 1-D region with a more external three-dimensional (3-D) region that would account for the convergence of the plasma to the wall.

The three length scales of the model are

(a) the collision mean free path, $\lambda_c=(T/m)^{1/2}/\nu_c$,

(b) the magnetic gyroradius, $\lambda_m=(Tm)^{1/2}/qB$,

(c) the Debye length, $\lambda_d=(T/4\pi q^2 N_*)^{1/2}$,

with $N_*=\Gamma_{x\infty}(m/T)^{1/2}$. We assume that the plasma is weakly collisional, with $\lambda_d \ll \lambda_c$, and we will let the magnetic length take any value from $\lambda_m \gg \lambda_c$ to $\lambda_m \ll \lambda_d$. The 1-D model is formally valid only if the curvature radius of the wall is much larger than λ_c.

Each of the scale lengths defines a dimensionless spatial variable:

$$\eta = x/\lambda_c, \quad \zeta = x/\lambda_m, \quad \xi = x/\lambda_d,$$

convenient for a particular plasma region. For the other plasma variables, we define the dimensionless magnitudes

$$n = \frac{N}{N_*}, \quad n_r = \frac{N_r}{N_*}, \quad \mathbf{v} = \frac{\mathbf{V}}{\sqrt{T/m}}, \quad t_r = \frac{T_r}{T},$$

$$\phi = -\frac{qU}{T}. \tag{5}$$

Using variables (5), but keeping, for the moment, the spatial variable dimensional, Eqs. (1)–(4) become

$$\frac{d^2\phi}{dx^2} = \frac{n - n_r}{\lambda_d^2}, \tag{6}$$

$$t_r \ln n_r + \phi = \text{const}, \tag{7}$$

$$n = 1/v_x, \tag{8}$$

$$\left(v_x - \frac{1}{v_x}\right)\frac{dv_x}{dx} = \frac{d\phi}{dx} + \frac{v_y \sin\psi}{\lambda_m} - \frac{v_x}{\lambda_c}, \tag{9}$$

$$v_x \frac{dv_y}{dx} = \frac{v_z \cos\psi - v_x \sin\psi}{\lambda_m} - \frac{v_y}{\lambda_c}, \tag{10}$$

$$v_x \frac{dv_z}{dx} = -\frac{v_y \cos\psi}{\lambda_m} - \frac{v_z}{\lambda_c}. \tag{11}$$

This set of equations verifies

$$-\frac{\lambda_d^2}{2}\left(\frac{d\phi}{dx}\right)^2 + v_x + \frac{1}{v_x} + n_r t_r + \frac{\lambda_c^2 v_z \sin\psi\cos\psi + \lambda_c\lambda_m v_y \sin\psi + (\lambda_m^2 + \lambda_c^2)(x/\lambda_c)}{\lambda_m^2 + \lambda_c^2\cos^2\psi} = \text{const}, \tag{12}$$

that is related to the conservation of momentum in the **B** direction; particular versions of this equation for $\lambda_c = 0$ and for $\psi = \pi/2$ were used previously by Chodura[1] and Riemann,[2] respectively. Moreover, in regions where collisions can be neglected (i.e., $\lambda_c \to \infty$) the energy of the attracted species is also conserved,

$$(v_x^2 + v_y^2 + v_z^2)/2 - \ln v_x - \phi = \text{const}; \tag{13}$$

adding this last equation to Eq. (7) we have the conservation law of the plasma energy, $(v_x^2 + v_y^2 + v_z^2)/2 - \ln v_x + t_r \ln n_r = \text{const}$. Finally, in any region where $\lambda_d^2 d^2\phi/dx^2 \ll n$ the plasma is quasineutral and Eqs. (6) and (9) simplify to

$$n_r \simeq n, \tag{14}$$

$$\left(v_x - \frac{c_s^2}{v_x}\right)\frac{dv_x}{dx} = \frac{v_y \sin\psi}{\lambda_m} - \frac{v_x}{\lambda_c}, \tag{15}$$

with $c_s = \sqrt{1 + t_r}$. Then, Eqs. (10), (11), and (15) constitute a closed set that determines the velocity field **v**. The potential and density profiles are obtained subsequently from Eqs. (7), (8), and (14).

Formally, boundary conditions for Eqs. (6)–(11) at $x = -\infty$ cannot be known without matching the 1-D solution with the ''external'' 3-D solution. If the undisturbed plasma is at rest, it is plausible to take $\mathbf{v} \to \mathbf{0}$ at $x = -\infty$, but the values of n, n_r, and ϕ at $x = -\infty$ cannot be fixed, as Eqs. (7) and (8) make clear. Fortunately, for $\lambda_d \ll \lambda_c$, the plasma is quasineutral far from the wall, and the above condition on **v** is enough to obtain the solution at $-x \gg 1$. This asymptotic solution allows us to integrate Eqs. (6)–(11) from $-x \gg 1$ as an initial-value problem. The integration is straightforward except when singular points have to be crossed. These can be seen as sonic points of the plasma flow. Equations (9) and (15) define two sound velocities: $V_x = \sqrt{T/m}$ for the attracted species, and $V_x = C_s \equiv c_s\sqrt{T/m} \equiv \sqrt{(T + T_r)/m}$ for the quasineutral plasma; we will see that a third sound velocity, $V_x = C_s \cos\psi$, appears in the parametric limit $\lambda_c/\lambda_m \to \infty$. Points where $v_x = 1$, $v_x = c_s \cos\psi$, and $v_x = c_s$ will be called points A, C, and S, respectively, and for each of them, it has to be analyzed whether the plasma profiles are regular or singular; in this last case there will be a transition between two plasma regions.

Solutions of Eqs. (6)–(11) and their boundary conditions depend on five dimensionless parameters, $\Lambda_{cm} = \lambda_c/\lambda_m$, $\Lambda_{dm} = \lambda_d/\lambda_m$, ψ, ϕ_W, and t_r:

(i) The ratios Λ_{cm} and Λ_{dm}, with $\Lambda_{dm} \ll \Lambda_{cm}$ for weakly collisional plasmas, are both proportional to B. They measure the strength of **B** relative to the ambipolar and the space-charge electric field, i.e., the E field in the quasineutral and non-neutral regions, respectively. They will indicate whether the plasma motion in the incidence plane, Oxz, tends to be channeled by **B** or by **E**. In the next sections the plasma response is investigated in the three distinguished limits, Figs. 1(b)–1(d): $\Lambda_{cm} = O(1)$ and $\Lambda_{dm} = 0$, or weak B field; $\Lambda_{cm} = \infty$ and $\Lambda_{dm} = 0$, or intermediate B field; $\Lambda_{cm} = \infty$ and $\Lambda_{dm} \geqslant O(1)$, or strong B field.

(ii) As the incidence angle ψ increases, the directions of **E** and **B** diverge and the competition between both fields to govern the direction of the plasma motion is more evident. The $\mathbf{E} \times \mathbf{B}$ drift (along Oy) will also increase with ψ. The angle ψ will be taken in the interval $0 \leqslant \psi \leqslant \pi/2$; if $\pi/2 \leqslant \psi \leqslant \pi$ one must just make the transformation $\psi \to \pi - \psi$, $(v_x, v_y, v_z) \to (v_x, v_y, -v_z)$; and if $-\pi \leqslant \psi \leqslant 0$ the appropriate transformation is $\psi \to -\psi$, $(v_x, v_y, v_z) \to (v_x, -v_y, -v_z)$.

(iii) The wall potential, $\phi_W \equiv -qU_W/T > 0$, is assumed large enough to produce a space-charge sheath close to the wall. In any case, as ϕ_W appears only as boundary condition

(monotonic) solutions $\phi(x)$ are universal for any ϕ_W.

(iv) The temperature ratio, $t_r = T_r/T$, affects mainly the sonic conditions.

III. INTERMEDIATE *B* FIELD: $\Lambda_{cm}\to\infty$, $\Lambda_{dm}\to 0$

This doubly distinguished limit leads to the model of Chodura but with the inclusion of the third, collisional region. The triple structure consists of the (collisional, *B* channeled) presheath, the Chodura layer, and the (unmagnetized) sheath, as sketched in Fig. 1(c). The equations of each region are obtained scaling appropriately the spatial variable in Eqs. (6)–(11), and taking then the asymptotic limits $\Lambda_{cm}\to\infty$ and $\Lambda_{dm}\to 0$. Thus the presheath corresponds to use $\eta = x/\lambda_c$, and its velocity field is given by

$$v_x + \frac{c_s^2 \cos^2\psi}{v_x} + \eta = \text{const}, \quad v_y = 0, \quad v_z = v_x \tan\psi; \tag{16}$$

the spatial profile $v_x(\eta)$ is readily obtained from the first equation, with $v_x \leqslant c_s \cos\psi$. This solution represents a classical, collisional presheath with the plasma moving along the *B* lines. The presheath extends from $\mathbf{v}\simeq\mathbf{0}$ until the sonic point (point C)

$$\mathbf{v}_C = (c_s\cos\psi, 0, c_s\sin\psi), \tag{17}$$

where $v_x(\eta)$ presents a turning point: $dv_x/d\eta|_C = \pm\infty$. Close to point C it is $dv_x/dx \sim 1/\lambda_m \gg 1/\lambda_c$, indicating that the plasma enters a steeper region of scale λ_m, the Chodura layer, that is both collisionless and quasineutral. The equations for this layer can be found in Refs. 1 and 2. They consist of Eqs. (12), (13), and (15) with $\zeta = x/\lambda_m$ as a convenient variable,

$$\begin{aligned} &\left(v_x + \frac{c_s^2}{v_x}\right)\cos\psi + v_z\sin\psi = 2c_s, \\ &\frac{v_x^2+v_y^2+v_z^2}{2} - c_s^2\ln\frac{v_x}{c_s\cos\psi} = \frac{c_s^2}{2}, \\ &\zeta\sin\psi = \int \frac{v_x^2 - c_s^2}{v_x v_y}\,dv_x. \end{aligned} \tag{18}$$

The Chodura layer extends from point C (placed at $\zeta_C = -\infty$) to the second singular/sonic point: point S, placed at

$$v_{xS} = c_s, \tag{19}$$

where $dv_x/d\zeta = \pm\infty$. Close to point S, it is $dv_x/dx \sim 1/\lambda_d \gg 1/\lambda_m$, indicating the transition to the space-charge sheath (where $v_y = v_{yS}$, $v_z = v_{zS}$). In the sheath scale, $\xi = x/\lambda_d$, the sheath verifies the well-known equations

$$\begin{aligned} &\phi - \phi_S = \frac{v_x^2 - c_s^2}{2} - \ln\frac{v_x}{c_s}, \\ &\frac{1}{2}\left(\frac{d\phi}{d\xi}\right)^2 = v_x + \frac{1}{v_x} + \frac{t_r}{c_s}\exp\frac{\phi_S - \phi}{t_r} - 2c_s, \end{aligned} \tag{20}$$

and the calculation of $\phi(\xi)$ is reduced to a quadrature.

Solutions for different incidence angles are displayed in Figs. 2(a)–2(e). The velocity fields, Figs. 2(a) and 2(b), show the evolution of the plasma flow in the three regions with the gentle transitions at points C and S. Clearly, the quasineutral region of plasma acceleration consists of both the presheath and the Chodura layer. The relative importance of each of

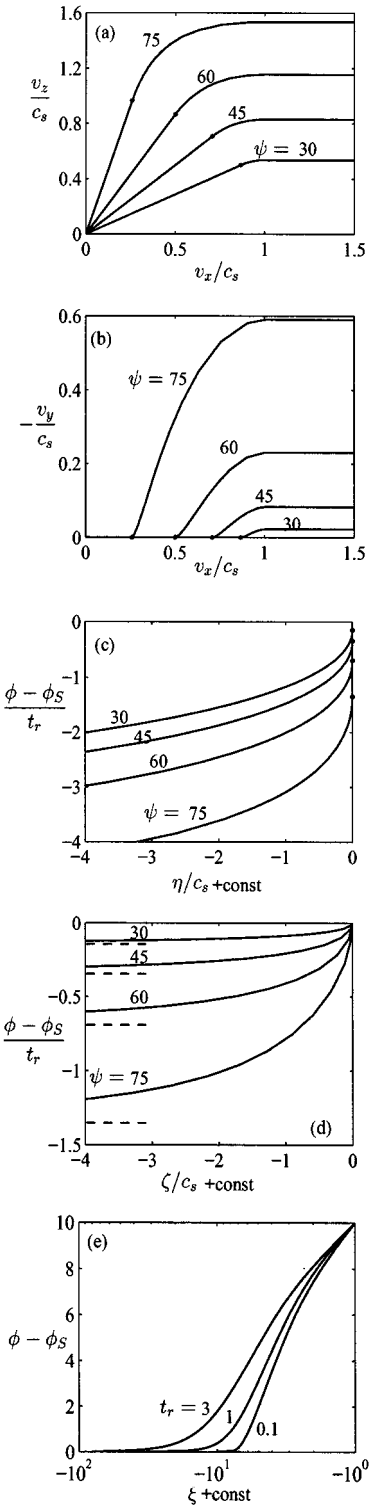

FIG. 2. Intermediate *B* field: $\Lambda_{cm}\to\infty$ and $\Lambda_{dm} = 0$. Plasma response in the three subregions. In (a)–(d): ψ(in degrees) = 30, 45, 60, and 75. In (e): $t_r = 0.1$, 1, and 3, and $\phi_W \leqslant 10$. Point S is at $v_x/c_S = 1$. The dot in (a)–(c) indicates point C. Dashed lines in (d) represent the asymptotic value $\phi = \phi_C$. For $\psi\to 90°$, it is $v_{yS}/c_s \simeq \sqrt{-\ln\cos^2\psi}$ and $v_{zS}/c_s \to 2$.

them depends on the angle of incidence: The Chodura layer disappears when $\psi \to 0$ and tends to be the whole quasineutral region when $\psi \to 90°$. The spatial profiles of the electrostatic potential in the three scales of this model can be compared in Figs. 2(c)–2(e). A complete view of the disturbance region is given by Fig. 2(c) where the collisional scale is used. Figure 2(d), first, and Fig. 2(e), then, provide local details of the potential jumps observed in the larger scales. The conclusion is that the characteristic extension of the perturbed (quasineutral) region $\Delta_{\rm qr}x$ is λ_c and not λ_m (or λ_d). Chodura and Riemann, who missed the *B*-aligned presheath, showed the potential in the intermediate scale λ_m, like Fig. 2(d). In that scale, the presheath cannot be reproduced and we just see that $\phi(\zeta)$ becomes flat at $\zeta \to -\infty$, as if there was no presheath structure.

The total potential drop in the quasineutral region $\Delta_{\rm qr}\phi$ includes contributions from the presheath and the Chodura layer, but its exact value cannot be known within the 1-D model. If we consider that the disturbance region extends to a point with typical speed v_∞, or $v_{x\infty}=v_\infty \cos\psi$, we have, from Eqs. (7), (8), and (14),

$$\frac{\Delta_{\rm qr}\phi}{t_r}=\ln\frac{c_s}{v_{x\infty}}=-\ln\cos\psi+\ln\frac{c_s}{v_\infty}, \tag{21}$$

where the two terms of the right-hand side correspond to the Chodura layer, $\phi_S-\phi_C$, and the presheath. The relation $v_\infty(\psi)$ comes from considerations external to this model, but the characteristics of the presheath suggest a weak dependence of v_∞ on ψ, and $\ln(c_s/v_\infty)=O(1)$.

This three-scale analysis has shown that the Chodura layer occupies an intermediate place between the two classical regions. The role of the Chodura layer is to drift the plasma from the *B*-aligned motion at the presheath to the *E*-aligned motion at the sheath; only in the Chodura layer the velocity field is 3-D, with both transversal and $\mathbf{E}\times\mathbf{B}$, self-induced drifts. Whether the Chodura layer is considered a ''presheath'' or a ''sheath,'' is just a question of the observer: it is a very thin sheath in the presheath scale ($\eta_S-\eta_C\simeq 0$), semi-infinite in its own scale ($\zeta_C\to-\infty$), and impossible to reproduce in the scale of the space-charge sheath. Indeed, the three length scales are characterizing the size of the electric field in each plasma region: **E** is inversely proportional to the local length scale. Thus in the presheath, the weak ambipolar *E* field can provide only a small acceleration to the plasma along the *B* lines. At point C, the increment in electric field is such that **E** can compete with **B** in the Chodura layer. At point S, a new change in **E** makes the electric field dominant in the sheath. Therefore points C and S are characterized by two common properties: both of them (i) are singular points of the plasma equations, and (ii) announce changes on the plasma dynamics due to changes on the magnitude of **E**. These similarities will be confirmed by the other two submodels.

The triple structure with transitions at points C and S is unique for a plasma that is quiescent ''at infinity.'' The matching with the presheath has demonstrated that there is no other choice for the entrance to the Chodura layer than sonic point C: On the one hand, the presheath, Eq. (16), exists only for $v_x \leqslant c_s \cos\psi$, and, on the other hand, the Chodura layer, for a plasma that enters the layer parallel to **B**, is restricted to $c_s \cos\psi \leqslant v_x \leqslant c_s$. This is the same kind of well-known proof that demonstrates that sonic point S is the only possible transition to the space-charge sheath. A different case is the one discussed in Refs. 4 and 5: the inclusion of an external *E* field parallel to the wall modifies certainly the plasma dynamics and structure.

IV. WEAK *B* FIELD: $\Lambda_{cm}=O(1)$, $\Lambda_{dm}\to 0$

This limit leads to the model proposed by Riemann.[2] Now there are only two length scales in the equations: $\lambda_c(\sim\lambda_m)$ and λ_d. Then the plasma recovers a classical double-structure consisting of presheath and sheath, Fig. 1(b). There is no Chodura layer in this model and point C, Eq. (17), disappears as singular point of the plasma equations: the former *B*-aligned presheath plus Chodura layer are merged now into a single quasineutral region, affected by both collisional and *B*-drift effects. The equations of this region are obtained from Eqs. (10), (11), and (15), using η as dimensionless spatial variable, and imposing $\mathbf{v}=\mathbf{0}$ at $\eta=-\infty$. The presheath extends now until point S, Eq. (19), where $dv_x/d\eta|_S=\pm\infty$, indicating the transition to the unmagnetized Debye sheath, Eqs. (20). The presheath equations must be integrated numerically. The asymptotic behavior of the three-component velocity field at $-\eta \gg 1$ is[2]

$$\mathbf{v}=-\frac{c_s^2}{\eta}\frac{1}{\Lambda_{cm}^2+1}\,(1+\Lambda_{cm}^2\cos^2\psi,\ -\Lambda_{cm}\sin\psi,\Lambda_{cm}^2\sin\psi\cos\psi)+\mathbf{O}(\eta^{-3}). \tag{22}$$

It corresponds to a diffusive motion, dominated by collisions, when the inertia term in Eq. (4), $\mathbf{V}d\mathbf{V}/dx$, is neglected. The integration of Eqs. (10), (11), and (15), with Eq. (22) as the ''initial'' condition, is straightforward with a standard Runge–Kutta routine for any Λ_{cm} and ψ, including $\psi=90°$, a regular case in this model. Riemann reported that inertial effects, of order η^{-3} in Eq. (22), must be taken into account to have a suitable ''initial'' condition when $\Lambda_{cm} \gg 1/\cos\psi$. This is not our conclusion: Eq. (22) has been used with satisfactory results for Λ_{cm} up to 10^4. The accuracy of the numerical solutions was checked both with the conservation law (12), and by comparing solutions with different ''initial'' values of η; we also checked that the inclusion of the $O(\eta^{-3})$ terms in Eq. (22) brought no difference.

Figures 3(a)–3(d) and 4(a)–4(d) illustrate the evolution of the velocity field and the potential profiles: $(\phi-\phi_S)/t_r=\ln(v_x/c_s)$, in the complete range of ψ and Λ_{cm}, including the comparison with the $\Lambda_{cm}=\infty$ model. Relevant properties of the velocity field are (i) magnetic effects on the plasma flow are negligible when $\Lambda_{cm}\ll 1$, as could be expected; (ii) the $\mathbf{E}\times\mathbf{B}$ drift starts now at $\mathbf{v}=0$, instead of at $v_{x0}=c_s$, but the final values v_{yS} are not very different in Figs. 2(b) and 4(b); (iii) for ψ not close to grazing incidence, v_{yS} is not monotonic with Λ_{cm}, presenting a maximum for $\Lambda_{cm}\sim 1$; (iv) when $\Lambda_{cm}=O(1)$ the differences between $\psi=75°$ and $\psi=90°$ are quite small (when $\Lambda_{cm}=\infty$ and large incidence angle, it is $v_{yS}\sim\sqrt{-\ln\cos^2\psi}$); and (v) v_{zS} behaves differ-

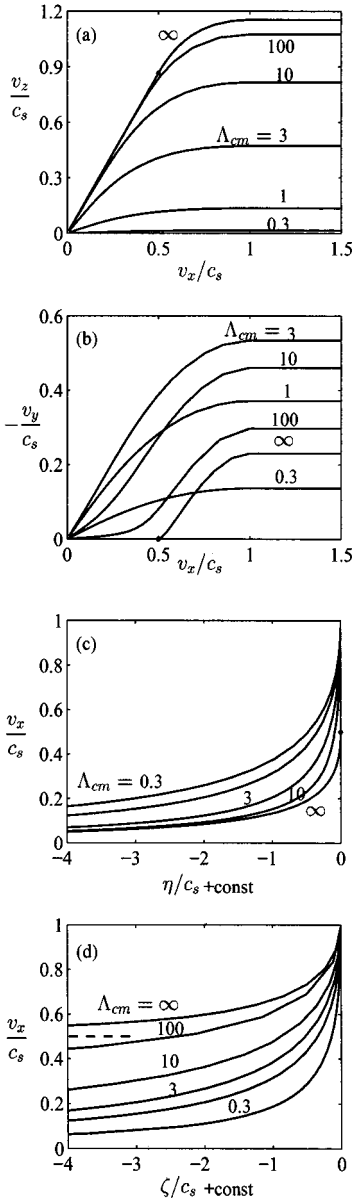

FIG. 3. Weak B field: $\Lambda_{cm}=O(1)$ and $\Lambda_{dm}=0$. Plasma response for $\psi=60°$ and $\Lambda_{cm}=0.3$, 1, 3, 10, 100, and ∞. Potential profiles are obtained from $(\phi-\phi_S)/t_r=\ln(v_x/c_s)$. For $\Lambda_{cm}=\infty$ (intermediate B case) in (a) and (c), point C is marked by a dot; in (c), the Chodura layer is the discontinuity, $\phi_S-\phi_C$; in (d), the dashed line is the asymptotic value: $\phi(\zeta=-\infty)=\phi_C$ and the B-aligned presheath cannot be reproduced.

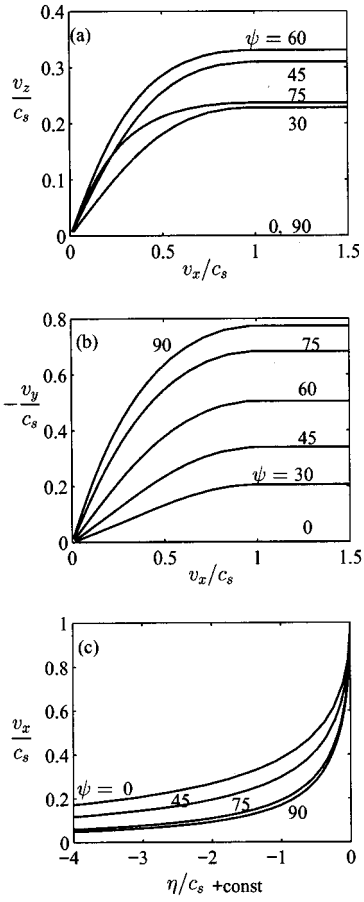

FIG. 4. Weak B field: $\Lambda_{cm}=O(1)$ and $\Lambda_{dm}=0$. Plasma response for $\Lambda_{cm}=2$ and several ψ(in degrees).

ently with ψ in Figs. 2(a) and 4(a). Except for $\psi\simeq 90°$, an adequate estimate of the dependence of v_y/v_x and v_z/v_x on ψ and Λ_{cm} can be obtained from Eq. (22).

For angles close to grazing incidence: $\cos\psi \ll 1$, Riemann found that the characteristic extension of the presheath, $\Delta_{qr}x$, was of the order of λ_m. When $\cos\psi\sim 1$, the scaling is certainly not that: Figs. 3(c) and 4(c) show that $\Delta_{qr}x$ is proportional to λ_c, for any Λ_{cm}, or, to be more precise, it goes from $\Delta_{qr}x\sim\lambda_c$, when $\Lambda_{cm}\leqslant O(1)$, to $\Delta_{qr}x\sim\lambda_c\cos^2\psi$, when $\Lambda_{cm}\gg 1/\cos\psi$.

In Figs. 3(a) and 3(b) we can see how the presheath approaches asymptotically the B-aligned presheath plus Chodura layer structure, when $\Lambda_{cm}\to\infty$. As the two submodels are derived from the general model of Sec. II, it is clear that the model of Riemann must yield the triple structure of the intermediate-B case when $\Lambda_{cm}\to\infty$. However, Riemann recovered only the Chodura layer because he did not apply the required two-scale analysis: He normalized the plasma equations using the ζ scale exclusively. In Figs. 3(c) and 3(d), we can compare the potential profiles in the two scales, $\phi(\eta)$ and $\phi(\zeta)$. For Λ_{cm} finite both of them yield the entire quasineutral region, but, when $\Lambda_{cm}\to\infty$, the two displays do not give the same information, only Fig. 3(c) reproduces completely the transition to the two subregions. [Figure 3(c) is also the most convenient to visualize correctly the presheath evolution with B (when λ_c is kept fixed), because ζ in Fig. 3(d) is already including B in its definition.] Point C is well defined only for $\Lambda_{cm}\to\infty$. Riemann, to compare his model with the Chodura layer, used, with Λ_{cm} finite, approximate equations that are singular at point C: this procedure is more confusing than clarifying because that singularity is fictitious in his model.

The solution of the presheath for $\psi=90°$ does not pose any difficulty. We can either integrate Eqs. (10) and (15), or follow the method of Behnel and Riemann: taking v_y from Eq. (12) and inserting it in Eq. (15) we just have to integrate

$$\left(v_x-\frac{c_s^2}{v_x}\right)\frac{dv_x}{d\zeta}=-\frac{v_x}{\Lambda_{cm}}+v_y$$
$$=-\frac{1}{\Lambda_{cm}}\left(2v_x+\frac{c_s^2}{v_x}\right)-\left(1+\frac{1}{\Lambda_{cm}^2}\right)\zeta. \tag{23}$$

As numerical solutions are increasingly difficult to obtain for larger Λ_{cm} and the Chodura model cannot be used with $\psi=90°$, our interest here is to obtain an approximate analytical solution of Eq. (23), valid for $\Lambda_{cm}\gg 1$. Keeping only the dominant terms in Eq. (23), it is readily seen that this solution is

$$\frac{v_x}{c_s}\simeq\frac{1}{\Lambda_{cm}}\sqrt{\frac{\pi}{2}}\exp\frac{\zeta^2}{2c_s^2}\operatorname{erfc}\left(-\frac{\zeta}{\sqrt{2}c_s}\right), \tag{24}$$

for $v_x/c_s\ll 1$. This expression shows two stages in the presheath: a collision-dominated part for $-\zeta\gg O(1)$, with $-v_y\sim v_x\Lambda_{cm}\sim -1/\zeta$; and a collisionless one for $\zeta\gg O(1)$, with $v_x\Lambda_{cm}\sim\exp(\zeta^2/2c_s^2)$ and $-v_y\sim\zeta$. Then v_x/c_s becomes $O(1)$ when $\zeta\sim -v_y\sim c_s\sqrt{\ln\Lambda_{cm}}\gg 1$, and the approximate solution to Eq. (23), for $v_x/c_s=O(1)$, is

$$2c_s^2\log v_x-v_x^2\simeq\zeta^2+\text{const}. \tag{25}$$

In this thin, final stage, inertial effects on v_x carry the plasma to singular point S.

Figures 5(a)–5(d) compare exact, numerical solutions with Eq. (24). When Eq. (25) is matched with Eq. (24), differences with the exact solution are insignificant for $\Lambda_{cm}>30$. Solution (24) confirms that the final $\mathbf{E}\times\mathbf{B}$ velocity, Figs. 5(b), behaves as

$$v_{yS}/c_s\simeq\sqrt{\ln\Lambda_{cm}^2},$$

a result already noticed by Riemann. However, Riemann's assertion that $\Delta_{qr}x\sim\lambda_m$, for the presheath extension, has to be limited to $\Lambda_{cm}=O(1)$. Figures 5(c) and 5(d) show that $\Delta_{qr}x$ depends strongly on Λ_{cm} when $\psi\simeq 90°$: it goes from $\Delta_{qr}x\sim\lambda_c$, when $\Lambda_{cm}\ll 1$, to

$$\Delta_{qr}x\sim\lambda_m/\sqrt{\ln\Lambda_{cm}^2},$$

when $\Lambda_{cm}\gg 1$. This last scaling law is obtained evaluating, with Eq. (24), the distance between ϕ_S and another fixed potential, Fig. 5(d). For grazing incidence, the considerations on Eq. (21) for the total potential drop in the quasineutral region are less reliable. Hence we are not sure that large $\mathbf{E}\times\mathbf{B}$ drifts mean large potential drops,[2] but they certainly mean large E fields (that is short presheaths): $E\propto 1/\Delta_{qr}x\propto v_{yS}$, according to the above scaling laws.

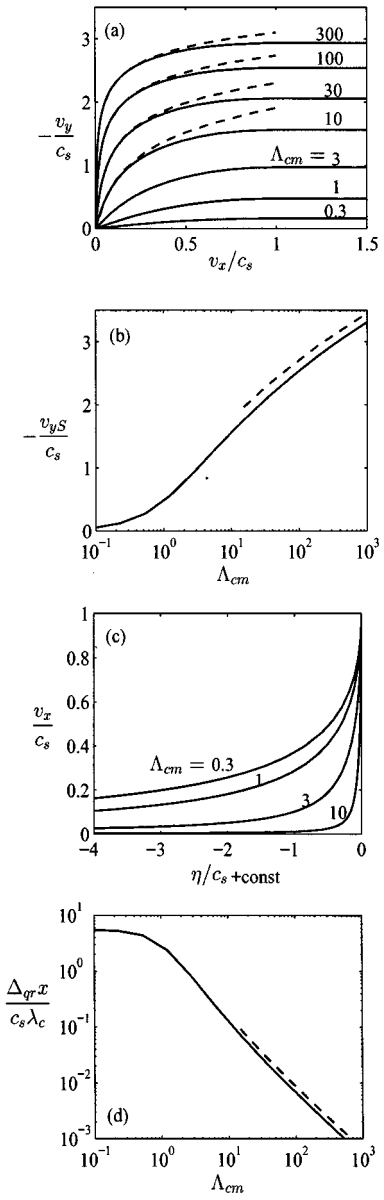

FIG. 5. Weak B field: $\Lambda_{cm}=O(1)$ and $\Lambda_{dm}=0$. Plasma response for $\psi=90°$. Dashed lines correspond to the approximate solution (24). In (d) $\Delta_{qr}x$ represents the distance between $\phi=\phi_S$ and $\phi=\phi_S-2t_r$.

V. STRONG B FIELDS: $\Lambda_{cm}\to\infty$, $\Lambda_{dm}\geqslant O(1)$

When Λ_{dm} is taken nonzero, the two scales of the plasma equations are λ_c and $\lambda_d\sim\lambda_m$. If we depart from the model of Chodura, we see that point S disappears as a singular point of the plasma equations: The Chodura layer merges with the Debye sheath to form a single, collisionless region where space-charge and magnetic effects compete. However, point C does not disappear and separates now the collisional, B-channeled presheath, Eq. (16), from the partially magnetized sheath, Fig. 1(d). Using ξ (or ζ) as spatial variable and taking then the limit $\Lambda_{cm}\to\infty$ in Eqs. (6)–(11), the equations of the sheath are

$$\frac{d^2\phi}{d\xi^2}=\frac{1}{v_x}-n_{rC}\exp\frac{\phi_C-\phi}{t_r},$$
$$\left(v_x-\frac{1}{v_x}\right)\frac{dv_x}{d\xi}=\frac{d\phi}{d\xi}+\Lambda_{dm}v_y\sin\psi,$$
$$v_x\frac{dv_y}{d\xi}=\Lambda_{dm}(v_z\cos\psi-v_x\sin\psi), \tag{26}$$
$$v_x\frac{dv_z}{d\xi}=-\Lambda_{dm}v_y\cos\psi.$$

Boundary conditions at point C: $\xi_C=-\infty$, are

$$\mathbf{v}_C = c_s(\cos\psi, 0, \sin\psi), \quad d\phi/d\xi|_C \simeq 0, \quad n_{rC} = 1/v_{xC}.$$

For $\Lambda_{cm} \to \infty$, the equation of conservation of momentum along **B**, Eq. (12), becomes

$$v_x \cos\psi + v_z \sin\psi + \left[\frac{1}{v_x} + t_r n_r - \frac{1}{2}\left(\frac{d\phi}{d\xi}\right)^2\right]\cos\psi = 2c_s. \tag{27}$$

This equation and Eq. (13) for the conservation of energy can substitute Poisson's equation in Eqs. (26), or instead, they can be used to check the accuracy of the numerical integration.

For $\Lambda_{dm} \ll 1$, we expect the magnetized sheath to resemble the Chodura layer plus Debye sheath structure of $\Lambda_{dm} = 0$. In the opposite limit: $\Lambda_{dm} \to \infty$, the solution to Eqs. (26) is

$$\mathbf{v} \simeq v(\cos\psi, 0, \sin\psi),$$

$$\phi - \phi_C = (v^2 - c_s^2)/2 - \ln(v/c_s), \tag{28}$$

$$\frac{\cos\psi}{2}\left(\frac{d\phi}{d\xi}\right)^2 = v + \frac{1}{v} + \frac{t_r}{c_s}\exp\frac{\phi_C - \phi}{t_r} - 2c_s,$$

that for $v \geqslant c_s$ reduces the calculation of $\phi(\xi)$ to a quadrature. Equations (28) represent a Debye sheath that is *B* channeled as the presheath. Its structure is identical to the *E*-channeled sheath of the limit $\Lambda_{dm} = 0$, Eqs. (20), except that now the plasma is accelerated by the component of **E** parallel to **B**. Observe that point *C* behaves for $\Lambda_{dm} \to \infty$ exactly like point *S* for the zero *B*-field case.

When $\Lambda_{dm} = O(1)$, the velocity field is 3-D and Eqs. (26) must be integrated numerically. In the Appendix we analyze their asymptotic behavior around point C that will be used as the ''initial'' condition for their integration. But a new problem can appear: Eqs. (26) are singular at $v_x = 1$ (point A), so depending on $v_{xC} \equiv c_s \cos\psi$ being larger or smaller than 1, point A is either a regular point of the presheath or a singular point of the sheath equations, respectively. The two cases are discussed separately.

A. One-mode sheath: $\tan^2\psi \leqslant t_r$

This condition is equivalent to $v_{xC} > 1$ and the sheath equations are regular from point C on. In the Appendix we show that, in this case, there is a unique mode that departs from point C: Writing $\mathbf{v} = \mathbf{v}_C + \mathbf{v}_1'$ and $\phi = \phi_C + \phi_1'$, its asymptotic behavior for $-\zeta \equiv -\Lambda_{dm}\xi \gg 1$ is [Eqs. (A6) and (A7)]

$$\mathbf{v}_1'(\zeta) = a\left(\frac{\cos\psi}{\zeta^2}, \frac{2c_s\sin\psi}{\zeta^3}, \frac{\sin\psi}{\zeta^2}\right),$$

$$\phi_1'(\zeta) = a\,\frac{t_r}{c_s\zeta^2}, \tag{29}$$

$$a = 6(c_s^3\sin^2\psi + \Lambda_{dm}^2 t_r^2\cos\psi)$$

[for $\Lambda_{dm} = O(1)$, we use ζ or ξ, indistinctly, according to convenience]. Departing from Eq. (29) the integration of Eqs. (26) from point C to the wall is straightforward. In the limits $\Lambda_{dm} = 0$ and $\Lambda_{dm} = \infty$, Eq. (29) recovers the asymptotic behavior, around C, of the Chodura layer and the *B*-channeled sheath, respectively.

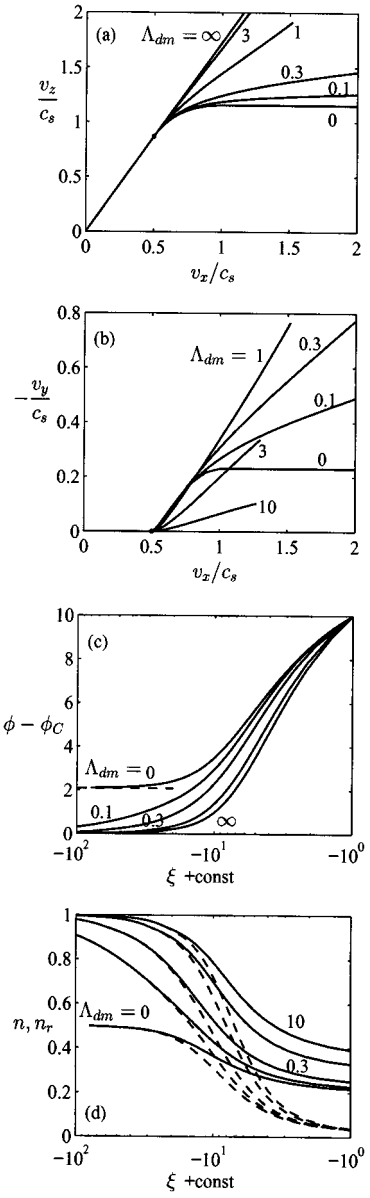

FIG. 6. Strong *B* field: $\Lambda_{cm} \to \infty$, $\Lambda_{dm} = O(1)$. Plasma response for $\psi = 60°$, $t_r = 3$, $\phi_W \leqslant 10$, and $\Lambda_{dm} = 0$ (intermediate-*B* case), 0.1, 0.3, 1, 3, 10, and ∞. Point C, separating presheath and sheath, is marked by a dot. The dashed line in (c) is the asymptotic value $\phi(\xi = -\infty) = \phi_S$ for $\Lambda_{dm} = 0$. Solid and dashed lines in (d) correspond to n and n_r, respectively.

Velocity profiles and sheath profiles are shown in Figs. 6(a)–6(d) and 7(a)–7(d). The sheath structure depends on three parameters: ψ, Λ_{dm}, and t_r, and is universal for any ϕ_W. Figures 6(a) and 6(b) show the continuous evolution of the velocity field from the three-region structure, for $\Lambda_{dm} = 0$, to the totally magnetized motion, for $\Lambda_{dm} = \infty$. In the plane of incidence the motion is practically *B* aligned for $\Lambda_{dm} > 1$. The differences with the case $\Lambda_{dm} = 0$ are more significant for the $\mathbf{E} \times \mathbf{B}$ drift, Figs. 2(b), 6(b), and 7(b). This presents a maximum for $\Lambda_{dm} = O(1)$, Fig. 6(b), when **E** and **B** are comparable, and becomes negligible for $\Lambda_{dm} \to \infty$, Eqs.

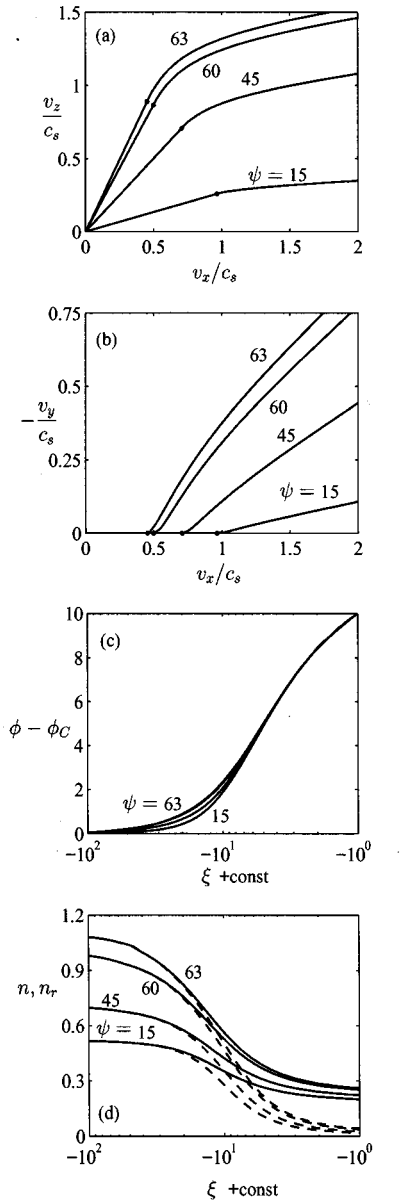

FIG. 7. Strong B field: $\Lambda_{cm}\to\infty$, $\Lambda_{dm}=O(1)$. Plasma response for $\Lambda_{dm}=0.3$, $t_r=3$, $\phi_W\leqslant 10$, and ψ(in degrees)$=15$, 45, 60, and 63. The case $\psi=63°$ corresponds to a two-mode sheath, with $\tan^2\psi>t_r$. Point C is marked by a dot. Solid and dashed lines in (d) correspond to n and n_r, respectively.

(28). A similar result was found in the weak-B case, but then **B** was compared with the ambipolar E field of the presheath. Potential, Figs. 6(c) and 7(c), and density profiles, Figs. 6(d) and 7(d), are shown in the scale of the sheath; they must be completed with Fig. 2(c) for the presheath. The difference $n-n_r$ measures the degree of non-neutrality of the sheath. The typical size of the sheath is given by the largest scale: λ_m for $\Lambda_{dm}\leqslant O(1)$, and λ_d for $\Lambda_{dm}\geqslant O(1)$. However, whereas the sheath presents a single scale for $\Lambda_{dm}\geqslant O(1)$, two scales are observed for $\Lambda_{dm}\ll 1$: λ_m for $v_x<c_s$ and λ_d for $c_s<v_x$, roughly. The dependence of the profiles on ψ lies almost exclusively in the entrance conditions to the sheath. The influence of t_r, not shown here, is similar to the case of an unmagnetized sheath, Fig. 2(e).

Only for $\Lambda_{dm}=0$, the partially magnetized sheath splits into the Chodura layer and the unmagnetized sheath; point S does not exist for $\Lambda_{dm}\neq 0$. Observe that for $\Lambda_{dm}=0$, profiles in Figs. 6(c) and 6(d) go asymptotically to point S and not to point C: the Chodura layer cannot be reproduced in the ξ scale; the ζ scale is needed to observe the profile of the partially magnetized sheath to converge asymptotically to the Chodura layer plus unmagnetized sheath structure. The similarities between this behavior and the model of Riemann in the limit $\Lambda_{cm}=\infty$ are obvious.

B. Two-mode sheath: $\tan^2\psi>t_r$

Now we have $v_{xC}<1$ and point A is inside the sheath. The only way that the solution to Eqs. (26) be regular at $v_x=1$ is that condition

$$(d\phi/d\zeta+v_y\sin\psi)|_A=0, \tag{30}$$

that can make $dv_x/d\zeta|_A$ finite in Eqs. (26), be satisfied. This is going to be possible thanks to the onset of two modes at point C: In the Appendix, we demonstrate that when $v_{xC}<1$ the asymptotic solution around point C: $-\zeta\equiv-\Lambda_{dm}\xi\gg 1$ is a linear combination of two modes:

$$\mathbf{v}=\mathbf{v}_C+\mathbf{v}_1'+\beta\mathbf{v}_2', \quad \phi=\phi_C+\phi_1'+\beta\phi_2', \tag{31}$$

where the new mode, $\mathbf{v}_2'$ and ϕ_2', verifies Eqs. (A1) and (A5),

$$\mathbf{v}_2'(\zeta)=((1+c_s^2\kappa^2)\cos\psi,-c_s\kappa\sin\psi,\sin\psi)\exp\kappa\zeta,$$

$$\phi_2'(\zeta)=-\frac{c_s^2\sin^2\psi}{\cos\psi\Lambda_{dm}^2 t_r}\exp\kappa\zeta, \tag{32}$$

$$\kappa=\left(\frac{\Lambda_{dm}^2 t_r^2\cos\psi+c_s^3\sin^2\psi}{(1-c_s^2\cos^2\psi)\Lambda_{dm}^2 t_r c_s^2\cos\psi}\right)^{1/2}.$$

The free constant β in Eq. (31) gives the required degree of freedom to fulfill the regularity condition (30).

For $\Lambda_{dm}=0$ and $\Lambda_{dm}=\infty$ we know that β must be 0, because the decoupling of the two length scales yields Eq. (29) as the only asymptotic mode at point C, for any incidence angle, ψ. For any other Λ_{dm}, the practical verification that there exists a value of β that makes the sheath solution regular across point A is not easy. Points C and A are both singular, so any initial-value method starting from any of them eventually sets in an unbounded mode when the other singular point is approached. This problem is aggravated by two facts: (i) the two pair of asymptotic modes have very different spatial growth rates, and (ii), as Eqs. (26) are nonlinear, the linear superposition of modes, Eq. (31), is valid around point C, exclusively. We proceeded, then, by integrating Eqs. (26) from points C and A simultaneously, and looking for the ''initial'' conditions and the intermediate point that gave an optimum matching of the two side solutions. In the vicinity of point C we used Eqs. (31) as ''initial'' conditions with β as the free parameter. At point A we took v_{yA} as the only free ''initial'' condition: v_{zA}, $\phi_A-\phi_C$, and $d\phi/d\zeta|_A$ were obtained from Eqs. (13), (27), and (30). Then the position of the intermediate point and the two free parameters, β and v_{yA}, were chosen such that the numerical errors at the matching point were minima. This method

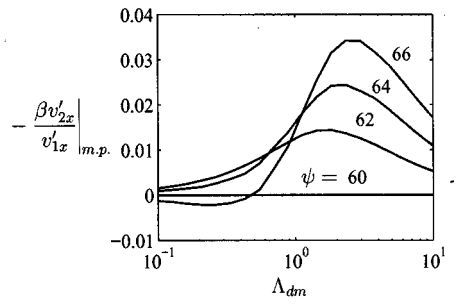

FIG. 8. Relative weight of the two linear modes that set in at point C, measured at the point (m.p.) where the solutions from C and A are matched.

proved to give adequate solutions when points C and A are close enough. As an example, we included in Fig. 7 the sheath solution for $\psi=63°$ and $v_{xC}\simeq 0.91$. Figure 8 displays estimations of the relative weight of the two modes for different values of Λ_{dm} and $1-v_{xC}$; it shows that the contribution of the second mode increases with $1-v_{xC}$, and is zero for Λ_{dm} equal to 0 and ∞. Therefore these numerical results confirm (i) the existence of regular solutions for the sheath when $\tan^2\psi > t_r$, and (ii) the continuity of these solutions across the parametric line $\tan^2\psi = t_r$. Unfortunately, the above shooting method is unsatisfactory when $1-v_{xC}$ is of order unity (when $1-v_{xC}>0.2$, roughly): unbounded modes and numerical errors impede the two side solutions to match smoothly at any intermediate point. This suggests that a different class of numerical techniques needs to be investigated for this case.

Finally, we want to comment that, also in this strong-B model, the transition between presheath and sheath can take place only at point C: the presheath admits transitions to the sheath at any $v_{x0}\leqslant v_{xC}$; but, for $v_{x0}<v_{xC}$, there is either no evanescent mode, if $v_{x0}\geqslant 1$, or one evanescent mode, if $v_{x0}>1$; in this last case, the solution becomes singular at $v_{x0}=1$, and cannot be continued to the wall.

VI. CONCLUSIONS

We have presented a model that reproduces the complete and continuous evolution of the plasma-wall transition with the magnetic field strength and direction. This transition depends on two dimensionless parameters, Λ_{cm} and Λ_{dm}. A triple structure consisting of (magnetized) presheath, Chodura layer, and (unmagnetized) sheath is well defined only in the double limit: $\Lambda_{cm}=\infty$ and $\Lambda_{dm}=0$, and then the Chodura layer is an intermediate region (with an intermediate scale) between the space-charge sheath and the (collisional and strongly magnetized) presheath. The model of Riemann is recovered for $\Lambda_{cm}=O(1)$ and $\Lambda_{dm}=0$ and shows a classical double structure: a presheath (that includes the former B-aligned presheath and Chodura layer) and an unmagnetized sheath. The other limit: $\Lambda_{cm}=\infty$ and $\Lambda_{dm}=O(1)$ leads to a double structure also, comprising a (B-aligned) presheath and a partially magnetized sheath (the combination of the former Chodura layer and unmagnetized sheath).

In relation to the model of Chodura, this paper makes contributions in the following aspects: (i) the presheath has a spatial structure that reflects the subsonic region of disturbance; (ii) potential drop and plasma acceleration in the presheath and Chodura layer are of the same order for $\cos\psi\sim 1$, and the differences among the three regions come from their different E fields; (iii) for ψ not close to 90°, the typical extension of the disturbance region is λ_c, and not λ_m; (iv) the matching with the presheath implies that the entrance to the Chodura layer is at sonic point C necessarily; and (v) points C and S present significant similarities.

In relation to the model of Riemann, our contributions lie in the following aspects: (i) for $\Lambda_{cm}\to\infty$, this model recovers the Chodura layer plus B-aligned presheath structure, and not just the Chodura layer; (ii) there is no point C in this model; (iii) the analysis of the entire range of ψ shows differences (in presheath extension and magnetic drifts, for instance) between $\cos\psi\ll 1$ and $\cos\psi\sim 1$; (iv) the integration of the presheath is straightforward and a generalized conservation law of momentum is derived; (v) for $\psi=90°$ we have obtained an approximate analytical solution (of the exact equations) valid for the near-singular case, $\Lambda_{cm}\gg 1$.

For the strong-B case, the partially magnetized sheath evolves from the Chodura layer plus the unmagnetized sheath for $\Lambda_{dm}=0$, to a B-aligned sheath for $\Lambda_{dm}=\infty$. An analysis of the linear modes that set in at the entrance of the sheath shows that they are a combination of cyclotron and space-charge modes. The dynamics of the sheath depends on the relative values of t_r and $\tan^2\psi$. For $\tan^2\psi\leqslant t_r$, the solution is obtained straightforwardly, departing from the unique asymptotic mode that is evanescent at point C. For $\tan^2\psi\geqslant t_r$, we are faced with a more difficult problem: the sheath equations are singular at an internal point (point A) and two asymptotic modes set in at point C. We have shown that the combination of the two circumstances leads to a unique and regular solution for the sheath. However, further investigations are required to find a reliable integration method when points C and A are not close enough, in particular, for large incidence angles.

The analysis of the transition points, C and S, through the three submodels has revealed their common characteristics. Mathematically each of them is a singular point of the plasma equations when a particular parametric limit is taken. When that limit is not imposed the singularity disappears: there is no point C when Λ_{cm} is finite, but there is no point S when Λ_{dm} is nonzero. Physically each of them brings along a change in the strength of the E field that modifies from one region to the other the physical process that dominates the plasma dynamics. The close relation between C and S is reaffirmed in the strong-B case: the main mode that sets in at point C evolves from a cyclotron mode when $\Lambda_{dm}=0$ to a space-charge mode when $\Lambda_{dm}=\infty$, showing that point C for $\Lambda_{dm}=\infty$ is equivalent to point S for $B=0$. Therefore even the characterization of the physical processes that become dominant at points C and S depends on the particular submodel. On the contrary, singular point A does present ''fundamental differences'' with C and S: it leads to neither a singular solution nor a change on the plasma dynamics.

The model we have presented is of application to both positive and negative wall potentials. The difference lies in the magnetic gyroradius λ_m that is relevant to the plasma

response: λ_m is the ion gyroradius for a cathodic wall ($U_W<0$), and the electron gyroradius for an anodic wall. As these gyroradii differ by a factor of the order of 10^2, the plasma structure is not ''symmetrical'' for U_W and $-U_W$.

ACKNOWLEDGMENTS

This work was supported by Ministerio de Educación y Ciencia of Spain (Project PB94-0417-C03-03).

APPENDIX: ASYMPTOTIC BEHAVIOR OF A MAGNETIZED SHEATH AROUND ITS ENTRANCE POINT

In this Appendix we look for solutions of the sheath equations that depart from point C. To better understand the physical modes represented by these solutions and to discuss how these modes change if the entrance to the sheath would be at a point different from C, we consider, for the moment, a general equilibrium point: $d/d\xi \equiv \Lambda_{dm} d/d\zeta \simeq 0$ of Eqs. (26):

$$v_{y0}=0, \quad v_{z0}=v_{x0}\tan\psi, \quad n_{r0}=1/v_{x0},$$
$$d\phi/d\xi|_0=0;$$

point C corresponds to $v_{x0}=v_{xC}\equiv c_s\cos\psi$.

Following the method used by Chodura to discuss the entrance to the Chodura layer when $\Lambda_{dm}\to 0$, we look for solutions of Eqs. (26) that depart from the above equilibrium point. The linearization of Eqs. (26) around this point is

$$\begin{aligned} &d^2\phi'/d\xi^2=-v_x'/v_{x0}^2+n_{r0}\phi'/t_r,\\ &(v_{x0}-1/v_{x0})dv_x'/d\xi=d\phi'/d\xi+\Lambda_{dm}v_y'\sin\psi,\\ &v_{x0}dv_y'/d\xi=\Lambda_{dm}(v_z'\cos\psi-v_x'\sin\psi),\\ &v_{x0}dv_z'/d\xi=-\Lambda_{dm}v_y'\cos\psi, \end{aligned} \tag{A1}$$

where the prime denotes the disturbance $v_x=v_{x0}+v_x'$ and so on. Assuming the time-independent disturbances proportional to $\exp(\kappa\zeta)\equiv\exp(\kappa\Lambda_{dm}\xi)$, with κ the dimensionless spatial rate, we obtain a biquadratic dispersion relation for κ,

$$t_r v_{x0}\Lambda_{dm}^2\kappa^2=\frac{(v_{x0}^2-c_s^2)(v_{x0}^2\kappa^2+\cos^2\psi)+v_{x0}^2\sin^2\psi}{(v_{x0}^2-1)(v_{x0}^2\kappa^2+\cos^2\psi)+v_{x0}^2\sin^2\psi} \tag{A2}$$

[here $t_r v_{x0}\Lambda_{dm}^2\equiv(\lambda_{dr}/\lambda_m)^2$, with $\lambda_{dr}=(T_r/4\pi q^2 N_{r0})^{1/2}$ the local Debye length of the repelled species, as used by Chodura]. The two roots of κ^2 in this equation are real for all values of the parameters. Therefore we have two pairs of linear modes and, for each pair, κ is either imaginary (and complex conjugate) or real (and of different sign). Modes with κ imaginary represent spatial fluctuations around the equilibrium point. Only modes with κ real and positive are evanescent at the equilibrium point (placed at $\zeta_0=-\infty$) and can produce the onset of the sheath.

For $\Lambda_{dm}\ll 1$ the approximate solutions of Eq. (A2) are[1]

$$\kappa^2\simeq\frac{v_{x0}^2-c_s^2\cos^2\psi}{v_{x0}^2(c_s^2-v_{x0}^2)}\equiv\frac{\sin^2\psi}{c_s^2-v_{x0}^2}-\frac{\cos^2\psi}{v_{x0}^2}, \tag{A3}$$

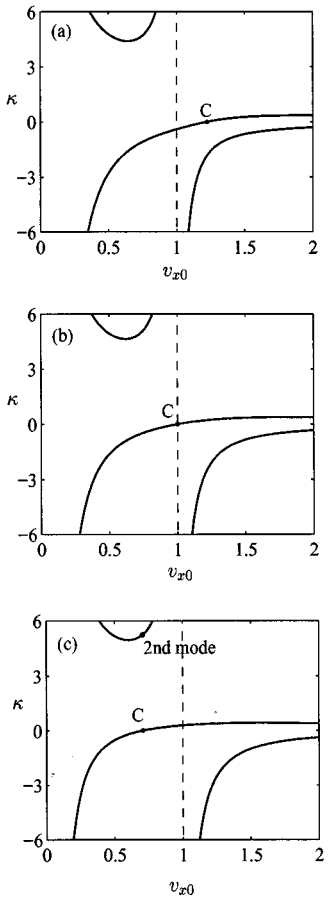

FIG. 9. Solutions of the dispersion relation for $\Lambda_{dm}=1$, $t_r=1$, and ψ(in degrees)=30(a), 45(b), and 60(c). At $v_{x0}=v_{xC}$, $\kappa=0$ is always a solution and yields a potentially evanescent mode; only in case (c), a second (exponentially) evanescent mode sets in.

$$(\Lambda_{dm}\kappa)^2\simeq\frac{v_{x0}^2-c_s^2}{t_r v_{x0}(v_{x0}^2-1)}\equiv\frac{n_{r0}}{t_r}-\frac{n_0}{v_{x0}^2-1}, \tag{A4}$$

whereas for $\Lambda_{dm}\gg 1$ the modes verify

$$\kappa^2\simeq\frac{v_{x0}^2-\cos^2\psi}{v_{x0}^2(1-v_{x0}^2)}\equiv\frac{\sin^2\psi}{1-v_{x0}^2}-\frac{\cos^2\psi}{v_{x0}^2}, \tag{A3$'$}$$

$$(\Lambda_{dm}\kappa)^2\simeq\frac{v_{x0}^2-c_s^2\cos^2\psi}{t_r v_{x0}(v_{x0}^2-\cos^2\psi)}\equiv\frac{n_{r0}}{t_r}-\frac{n_0}{v_0^2-1} \tag{A4$'$}$$

($v_0=v_{x0}/\cos\psi$). Equations (A3) and (A3$'$) represent a pair of oblique, cyclotron modes, and Eqs. (A4) and (A4$'$) correspond to a pair of space-charge modes. Figure 9 shows the solutions of Eq. (A2) for $\Lambda_{dm}=1$ and several incidence angles.

The solutions to Eq. (A2) have two properties that are of interest to us. For any Λ_{dm}:

(a) There is one pair of modes with κ^2 changing from positive to negative (through $\kappa^2\to\pm\infty$) at $v_{x0}=1$; this pair corresponds to Eqs. (A4) and (A3$'$) in the respective limits of Λ_{dm}. Therefore if $v_{x0}<1$, there is one mode in this pair that is evanescent. For the particular case $v_{x0}=v_{xC}$, the spatial rates of this pair are easy to obtain

$$(\Lambda_{dm}\kappa)^2=\frac{c_s^2-v_{xC}^2}{(1-v_{xC}^2)v_{xC}t_r}+\Lambda_{dm}^2\,\frac{v_{xC}^2-\cos^2\psi}{(1-v_{xC}^2)v_{xC}^2}. \qquad \text{(A5)}$$

(b) The second pair crosses from $\kappa^2>0$ to $\kappa^2>0$ when v_{x0} goes from $v_{x0}<v_{xC}$ to $v_{x0}>v_{xC}$. Therefore one mode of this pair changes from exponentially evanescent to oscillatory when the quasineutral point crosses point C. For $\Lambda_{dm}\to 0$ the evanescent mode is a cyclotron one, Eq. (A3), whereas for $\Lambda_{dm}\to\infty$, it is a space-charge mode, Eq. (A4′). Let us demonstrate now that the mode is potentially evanescent when $v_{x0}=v_{xC}$. We start making the ansatz that it behaves as

$$v_x'=a\zeta^{-m}\cos\psi+o(\zeta^{-m}),$$

for certain constants a and m to be found. Then Eqs. (A1) yield, for the other perturbation variables,

$$\mathbf{v}'\simeq a\left(\frac{\cos\psi}{\zeta^m},\frac{mv_{xC}\tan\psi}{\zeta^{m+1}},\frac{\sin\psi}{\zeta^m}\right),\quad \phi'\simeq a\,\frac{t_r\cos\psi}{v_{xC}\zeta^m}, \qquad \text{(A6)}$$

but the linear equations (A1) do not determine a and m. This task requires to consider the nonlinear perturbation terms in Eqs. (26). Instead of obtaining the next perturbation order of all these equations, we use the (exact) equation

$$\left(\frac{v_x}{\cos^2\psi}-\frac{c_s^2}{v_x}\right)\frac{dv_x}{d\zeta}=\Lambda_{dm}^2\,\frac{t_r}{n_r v_x}\,\frac{d}{d\zeta}\left(v_x\,\frac{d^2\phi}{d\zeta^2}\right)-v_x\,\frac{\sin\psi}{\cos^2\psi}\,\frac{d}{d\zeta}\left(v_x\,\frac{dv_y}{d\zeta}\right),$$

obtained directly from Eqs. (26). Expanding this last equation and using Eq. (A6) we have

$$m=2,\quad a=6(c_s^3\sin^2\psi+\Lambda_{dm}^2t_r^2\cos\psi). \qquad \text{(A7)}$$

The two contributions to κ and a in the right-hand sides of Eqs. (A5) and (A7) show that, for $\Lambda_{dm}=O(1)$, each mode combines cyclotron and space-charge effects.

In conclusion, for Λ_{dm} finite and nonzero we have:

(i) If $v_{xC}\geqslant 1$, Eqs. (A6) and (A7) give the unique spatial mode that sets in at point C, and this determines uniquely the sheath solution.

(ii) If $v_{xC}<1$, there is an additional mode that set in at point C and an extra condition is needed to determine the sheath profile. The spatial rate of this mode comes from Eq. (A5) with $\kappa>0$; $\mathbf{v}'$ and ϕ' are obtained from Eqs. (A1).

For $\Lambda_{dm}=0$ and $\Lambda_{dm}=\infty$, the scenario is simpler because the two scales ζ and ξ are uncoupled and, in each scale, there is only one pair of modes. Thus in the limit of Chodura, we have the cyclotron modes (A3) in the ζ scale that are monotonic in the range $c_s\cos\psi<v_{x0}<c_s$ (that is between points C and S); Chodura showed in this way the domain of existence of the Chodura layer. [Also the onset of the Debye sheath at point S, in the ξ scale, corresponds to a space-charge mode, of the type (A4), that is monotonic for $v_{x0}>c_s$.] In the opposite limit, $\Lambda_{dm}=\infty$, the behavior is different, the collisionless region is not constituted by two subregions: In the intermediate scale (ξ, now) only space-charge modes (A4′) can develop and these are monotonic from point C on; therefore, there is no transition to the thinnest scale ζ and cyclotron modes (A3′) are never observed.

[1] R. Chodura, Phys. Fluids **25**, 1628 (1982).
[2] K. U. Riemann, Phys. Plasmas **1**, 552 (1994).
[3] P. C. Stangeby, Phys. Plasmas **2**, 702 (1995).
[4] P. C. Stangeby and A. V. Chankin, Phys. Plasmas **2**, 707 (1995).
[5] I. H. Hutchinson, Phys. Plasmas **3**, 6 (1996).
[6] G. H. Kim, N. Hershkowitz, D. A. Diebold, and M. H. Cho, Phys. Plasmas **2**, 3222 (1995).
[7] U. Daybelge and B. Bein, Phys. Fluids **24**, 1190 (1981).
[8] A. B. DeWald, A. W. Bailey, and J. N. Brooks, Phys. Fluids **30**, 267 (1987).
[9] Y. Q. Tao, R. W. Conn, L. Schmitz, and G. Tynan, Phys. Fluids B **5**, 344 (1993).